

An assessment of the resolution limitation due to radiation-damage in x-ray diffraction microscopy

M. R. Howells,^{1,*} T. Beetz,¹ H. N. Chapman,² C. Cui,³ J. M. Holton,³ C. J. Jacobsen,^{3,1} J. Kirz,³ E. Lima,¹ S. Marchesini,² H. Miao,¹ D. Sayre,¹ D. A. Shapiro,^{3,1} and J. C. H. Spence^{3,4}

¹*Department of Physics, State University of New York, Stony Brook, NY 11794, USA*

²*Lawrence Livermore National Laboratory, 7000 East Ave., Livermore, CA 94550, USA*

³*Advanced Light Source, Lawrence Berkeley National Laboratory, 1 Cyclotron Rd., Berkeley, CA 94720 USA*

⁴*Department of Physics and Astronomy, Arizona State University, Tempe, AZ 85287-1504, USA*

X-ray diffraction microscopy (XDM) is a new form of x-ray imaging that is being practiced at several third-generation synchrotron-radiation x-ray facilities. Although only five years have elapsed since the technique was first introduced, it has made rapid progress in demonstrating high-resolution three-dimensional imaging and promises few-nm resolution with much larger samples than can be imaged in the transmission electron microscope. Both life- and materials-science applications of XDM are intended, and it is expected that the principal limitation to resolution will be radiation damage for life science and the coherent power of available x-ray sources for material science. In this paper we address the question of the role of radiation damage. We use a statistical analysis based on the so-called “dose fractionation theorem” of Hegerl and Hoppe to calculate the dose needed to make an image of a life-science sample by XDM with a given resolution. We conclude that the needed dose scales with the inverse fourth power of the resolution and present experimental evidence to support this finding. To determine the maximum tolerable dose we have assembled a number of data taken from the literature plus some measurements of our own which cover ranges of resolution that are not well covered by reports in the literature. The tentative conclusion of this study is that XDM should be able to image frozen-hydrated protein samples at a resolution of about 10 nm with “Rose-criterion” image quality.

Keywords: Coherent x-rays, diffraction imaging, radiation damage, dose fractionation, frozen-hydrated samples

INTRODUCTION

X-ray diffraction microscopy (XDM) is a new form of x-ray imaging that is now being practiced by the authors at the Advanced Light Source x-ray facility at Berkeley [1, 2]. Similar work has been done at the synchrotron-light sources at Brookhaven [3, 4], Argonne [5, 6] and the Spring 8 facility in Japan [7, 8]. The method works in both 2D and 3D and can be adapted for both life [4] and materials sciences. The images are generated in three steps; (1) diffraction patterns are recorded using coherent x-rays (just one for 2D or a tilt series for 3D) which provides the amplitudes of the diffracted wave field, (2) the phases of the wave field are obtained using variants of phase-retrieval algorithms developed in other branches of optics [9, 10, 11] and (3) the image is recovered by means of a Fourier transform.

This form of x-ray imaging was first suggested by Sayre [12] and first demonstrated at Brookhaven in 1999 by Miao, Charalambous, Kirz and Sayre [3]. The latter experiment achieved a resolution of 75 nm using 0.73 keV x-rays and subsequent 2D experiments have pushed that value down to 7 nm measured in the image [7]. Our own XDM experiments have been done in the energy region 0.5–0.8 keV while other workers have used energies up to 8 keV. Although all of the above-mentioned groups have achieved 3D imaging with test objects, the resolution in these experiments is still several times worse than in 2D.

Nevertheless the expansion of interest in the technique and the progress in developing its performance has been rapid and we are lead to investigate the fundamental limits to this form of microscopy. It appears that the limit for life-science samples will be set by radiation damage, while for more-radiation-hard materials-science samples it will be set by the coherent power of available x-ray sources.

In this paper we address the question of the role of damage in setting a resolution limit to life-science imaging by XDM. This is important because, XDM is expensive (it needs at least an undulator on a third-generation synchrotron source) and if it is to have a niche in which it delivers unique and useful results, then it must produce performance beyond the limits of other microscopes. In this work, we refer to the practice of fast freezing the sample and holding it at low temperature for imaging, as “cryo-protection”. Such protection is used, for example, by the Munich group in their “electron-cryotomography” system [13] which recently demonstrated a 3D resolution of 5-6 nm for biological samples of thickness 0.3-0.6 μm . Further analysis by the same group [14] has indicated that, although the resolution may eventually be improved by a factor of 2-3, the thickness is a hard limit caused by multiple scattering. Such a thickness limit would not apply to XDM so the question becomes: can XDM achieve good enough resolution to produce images with similar quality to cryoelectron tomography but of whole cells in

the 0.5 to say 5-10 μm size range? A more fundamental reason why the issue of resolution is important in these investigations is that the resolution achieved by the Munich group is beginning to enable protein molecules of known structure in the sample to be recognized. The potential for determining the way in which these proteins “dock” together and thus for throwing light on their function in molecular machines is an exciting general goal of these types of ultramicroscopy.

The question of calculating how much dose is *needed* for imaging in a given microscope at a given resolution and statistical accuracy is essentially a statistical calculation. Such calculations have been presented before for x-ray microscopy in general [15, 16, 17] and for XDM [1, 18, 19]. On the other hand the question of how much dose can the sample *tolerate* before unacceptable degradation occurs to images at a given resolution is not a matter of statistics but rather of radiation chemistry and biology. We thus arrive at two important quantities that we need to know about in order to estimate the dose-limited resolution, the *required dose for imaging* and the *maximum tolerable dose*. Obviously experiments can only be successful if the dose employed is greater than the required dose for imaging and less than the maximum tolerable dose.

In what follows we will use various techniques to estimate the required dose and the maximum tolerable dose. For the required dose we will use an estimation method based on the so-called dose fractionation theorem [20, 21] which we explain below. To use the theorem for a 3D diffraction experiment one needs to know the scattering strength of a single voxel. This cannot normally be measured but we will describe simple methods by which it can be calculated and will compare the dose-resolution scaling law that results with our own XDM measurements. The maximum tolerable dose cannot be estimated by a simple calculation so it needs to be inferred from experimental results. We discuss below various experiments by ourselves and others that may be able to provide information. Since no 3D images of biological samples have yet been made by XDM, we try to make the best use of results from other types of experiment, 2D XDM, x-ray and electron crystallography and conventional electron and x-ray microscopy. Using these methods we will make tentative estimates of the future capability of XDM based on the presently-available evidence.

THE DOSE FRACTIONATION THEOREM

The theorem that we will use to simplify our calculation of the required dose for imaging was first proved by Hegerl and Hoppe [20]. It states, “A three-dimensional reconstruction requires the same integral dose as a conventional two-dimensional micrograph provided that the level of (statistical) significance and the resolution are

identical”. The discussion provided by the originators of the theorem was largely in terms of a single voxel but, as pointed out by McEwan, Downing and Glaeser [21], the conclusion can be immediately generalized to a full 3D object by recognizing that conventional tomographic reconstructions are *linear* superpositions of the contributions of the individual voxels. A similar argument can be used to show that the theorem is applicable to XDM. McEwan et al also showed by computer simulations that the validity of the theorem could be extended to include experimentally realistic conditions of high absorption, signal-dependent noise, varying contrast and missing angular range.

We consider a single voxel of the type that we would reconstruct in a fully 3D experiment, which means one with the same width in all three dimensions. In order to apply the theorem to predict the “required dose for imaging”, we need to know the dose required in an XDM experiment on the *single voxel alone* for an interesting range of values of d . It would be extremely hard to do such a series of experiments in practice. However, since the one-voxel experiments are simple in principle, it is easy to obtain their results by theoretical analysis which is what we do below. We will study a voxel of size $d \times d \times d$ which corresponds to correct sampling for resolving a smallest spatial period of $2d$ in each coordinate direction (roughly similar to a Rayleigh resolution of d in standard microscopy).

To obtain the dose required for the one-voxel experiment we begin by calculating the x-ray coherent scattering cross section (σ_s) of the voxel for scattering into a detector with the right solid-angle collection to get the resolution d . This gives the dose required to get a given number of x-rays scattered by the voxel into the detector. The refractive index $\tilde{n} = 1 - \delta - i\beta$, the intensity absorption coefficient μ , and the complex electron density $\tilde{\rho}$ that we will need can be obtained from the tabulated optical constants as described, for example, in [22] equations 17, 18, 23 and 19 respectively.

CALCULATION OF THE COHERENT SCATTERING CROSS SECTION OF THE VOXEL

Suppose the voxel is of amplitude transparency T surrounded by empty space of transparency unity. The Babinet inverse of this scattering object is an aperture of transparency $1 - T$ in an opaque screen. Babinet’s Principle asserts that, outside the (small) area of the incident beam, the diffraction pattern of these two objects is the same. The diffracted intensity at distance z is most easily calculated for the second object [23] as follows:

$$I(x, y) = \frac{I_{\text{in}} |1 - T|^2 d^4}{\lambda^2 z^2} \text{sinc}^2\left(\frac{xd}{\lambda z}\right) \text{sinc}^2\left(\frac{yd}{\lambda z}\right).$$

The numerical aperture required to resolve a spatial

period $2d$ is $\lambda/(2d)$ so the full width of the detector in both x and y should be $w = \lambda z/d$. Thus

$$\begin{aligned} \frac{\sigma_s}{d^2} &= \frac{\text{scattered energy}}{\text{incident energy}} \cong \frac{I(0,0) w^2}{I_{\text{in}} d^2}, \\ &= \frac{I_{\text{in}} |1 - T|^2 d^4}{\lambda^2 z^2} \left(\frac{\lambda z}{d} \right)^2 \frac{1}{I_{\text{in}} d^2}, \\ &= |1 - T|^2, \end{aligned}$$

showing that $\sigma_s = |1 - T|^2 d^2$ which is in agreement with equation 23 of [24] for example, as well as being intuitively reasonable. To get the complex absorbcency, $1 - T$ in terms of the material properties of the voxel we use [22] equation (20) for the wave amplitude ψ :

$$\begin{aligned} \psi &= \psi_0 e^{-2\pi i \tilde{n} d / \lambda} = \psi_0 e^{-2\pi i (1 - \beta - i\delta) d / \lambda}, \\ &= \psi_0 e^{-2\pi i d / \lambda} e^{-2\pi \beta d / \lambda} e^{2\pi \delta d / \lambda}, \text{ whence} \\ T &= e^{-2\pi \beta d / \lambda} e^{2\pi \delta d / \lambda} \simeq 1 - 2\pi d (\beta + i\delta) / \lambda, \end{aligned}$$

where we have introduced the weak-phase-weak-amplitude approximation (which will usually be valid for a resolution element which is intrinsically small). Recasting this in terms of the complex electron density $\tilde{\rho}$, ([22] equation 19), we have:

$$|1 - T|^2 = (2\pi d)^2 |\beta + i\delta|^2 / \lambda^2 = d^2 r_e^2 \lambda^2 |\rho|^2,$$

and finally,

$$\sigma_s = |1 - T|^2 d^2 = r_e^2 \lambda^2 |\rho|^2 d^4. \quad (1)$$

Thus σ_s scales as the voxel size to the fourth power. As we will see this leads to an inverse fourth-power scaling of the dose with d . The scaling with wavelength is dominated by the λ -squared term, especially at wavelengths $\ll 2$ nm where the $\tilde{\rho}$ values of the light elements approach a constant value.

Equation (1) is important to our argument and we have checked it in various ways. Firstly, we took the scattering cross section of a single electron and summed it coherently over all the electrons in our voxel. Secondly we used literature calculations of the cross section of spherical particles of the same size as our voxel [25, 26]. The three expressions so obtained agreed with equation (1) up to a constant factor of order one. We may also argue that the contrast (C) between the voxel and vacuum scales as the thickness, i. e. as d . The Rose criterion (see later) says that the number of incident x-rays per unit area, N_0 , which is proportional to the dose, must satisfy $N_0 d^2 > 25/C^2$. Therefore, since C scales as d , N_0 scales as $1/d^4$.

RELATION BETWEEN FLUX DENSITY AND DOSE

Before proceeding to calculate the dose for our case we first make some definitions and show how the dose is

related to the number of incident particles per unit area. This relationship will be needed in order to compare published data from different sources. For x-rays of energy $h\nu$, we know that for any object (with density ε), the number of transmitted x-rays per unit area N at depth t due to an incident number per unit area N_0 is given by $N = N_0 \exp(-\mu t)$ whence the *energy* deposition per unit volume at the surface, $[\partial(Nh\nu)/\partial t]_{t=0}$, is $\mu N_0 h\nu$. Therefore the dose D (energy deposited per unit mass) is:

$$D = \mu N_0 h\nu / \varepsilon. \quad (2)$$

D will be in Gray (J/kg) if the other quantities are in MKS units. The last equation relates the incident particle flux density to the dose for given material parameters irrespective of d . Some numerical values for protein are given in Fig. 1.

In the case of illumination by an electron beam, the energy deposited per unit length of trajectory (and thence per unit volume) is given by the Bethe formula, (see for example equation 10.2 of [27]) which we have used for some of the entries in Fig. 4.

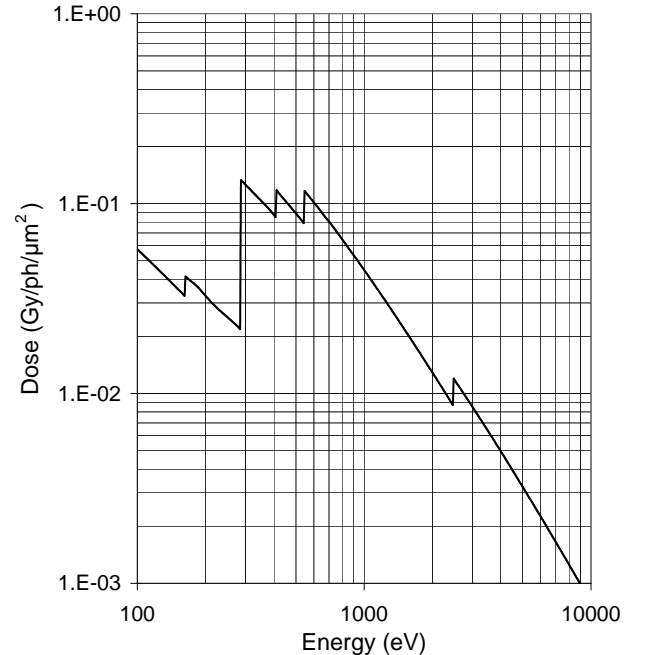


FIG. 1: The surface dose in Gray for an incident x-ray flux density of $1/\mu\text{m}^2$ for a range of x-ray energies. The material is taken to be protein of empirical formula $\text{H}_{50}\text{C}_{30}\text{N}_9\text{O}_{10}\text{S}_1$ and density 1.35 gm/cm^3

ESTIMATION OF THE DOSE AND CALCULATION OF THE REQUIRED IMAGING DOSE

We want to estimate the dose D (Gy) and the number of incident x-rays per unit area N_0 required to get a given number P of x-rays scattered into the detector from the given voxel (The choice of P will be determined by the statistical accuracy required from the measurement). The number of photons incident on the voxel is $N_0 d^2$ of which a fraction σ_s/d^2 will be scattered into the detector. Therefore the requirement is for $N_0 = P/\sigma_s$ which, from equations (1) and (2), leads to:

$$D = \frac{\mu P h \nu}{\varepsilon \sigma_s} = \frac{\mu P h \nu}{\varepsilon} \frac{1}{r_e^2 \lambda^2 |\rho|^2 d^4}, \quad (3)$$

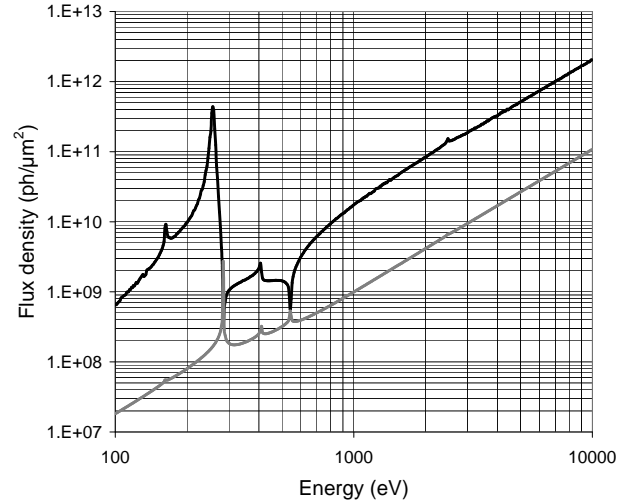
and

$$N_0 = \frac{P}{r_e^2 \lambda^2 |\rho|^2 d^4}. \quad (4)$$

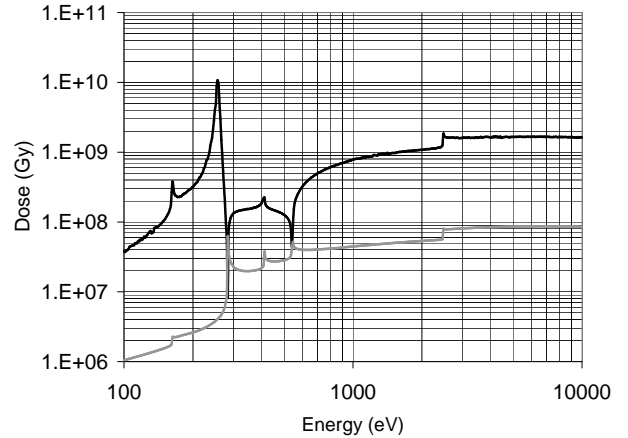
As examples we show the flux and dose curves (Fig. 2) for a protein sample of empirical formula $\text{H}_{50}\text{C}_{30}\text{N}_9\text{O}_{10}\text{S}_1$ and density 1.35 gm/cm^3 as a function of x-ray energy. The curves are for a voxel size (resolution) of 10 nm and statistical accuracy based on the Rose criterion [28]. The latter is an experimentally-based criterion for reliable detectability of a feature against background noise. The requirement is generally that the feature signal should be five times greater than the rms background noise. When the noise is the shot noise of the feature signal itself then it is conventional to set the particle count equal to 25. The flux curve (Fig. 2(a)) is dominated by the λ^{-2} scaling of the cross section. This argues for using the longest possible wavelength for these experiments. On the other hand the wavelength should be shorter than, say, a quarter to a half of the resolution so that the diffraction angle is not too large, and short enough that the sample is a weak absorber ($< 20\%$, say), so that data analysis can proceed on the basis of the Born approximation. Unlike the flux, the dose does not show strong energy dependence above about 1 keV. This is because the roughly $\lambda^{5/2}$ scaling of the absorption coefficient tends to cancel the wavelength dependence of $h\nu/\sigma_s$ in equation (3).

Equation (3) also allows the calculation of the “required imaging dose” as a function of resolution d . We have evaluated that for protein against a background of water for 1 keV and 10 keV as shown by the solid and dashed straight lines in Fig. 4. One can see that the change in dose from 1 keV to 10 keV is not very significant.

Also from (3) the resolution scaling of the dose is seen to be $1/d^4$ and is determined entirely by the cross section. Applying the dose fractionation theorem we may say that the *same dose* will be required to measure



(a)



(b)

FIG. 2: (a) The flux density and (b) the dose required to visualize a 10 nm cubic voxel of protein of empirical formula $\text{H}_{50}\text{C}_{30}\text{N}_9\text{O}_{10}\text{S}_1$ and density 1.35 gm/cm^3 against a background of water (black) and vacuum (gray) according to the Rose criterion.

the same $d \times d \times d$ voxel to the same statistical accuracy in a 3D tomography experiment. Hence, the inverse-fourth-power scaling with d , will also apply to a 3D sample.

It is important to note that the flux, predicted by Fig. 2 to be required for a 10 nm XDM experiment on protein against a background of water, needs to be delivered to the sample as a coherent x-ray beam. Part of the attraction of XDM is that such coherent x-ray beams are already available from undulators on current synchrotron-radiation sources such as the Advanced Light Source at Berkeley USA. For example our present experiments are done using exposure times of several tens of seconds per

view in a tomographic tilt series using a general-purpose beam line. The use of a purpose-designed beam line plus the soon-to-be-completed ALS upgrade would improve that by a factor of about a thousand.

MEASUREMENTS OF THE REQUIRED IMAGING DOSE

In order to test the calculations of the required imaging dose we have carried out the following series of measurements. Two-dimensional diffraction patterns were recorded using a series of exposure times that increased on a logarithmic grid. The patterns were analyzed by first taking an azimuthal average so as to produce a relation between diffracted signal and spatial frequency. A cut-off frequency was then determined from where the diffracted signal reached the noise floor of the detector. The exposure times were converted to dose units and the cut-off frequencies to spatial half-periods giving a relation between dose and resolution. One of these relationships, taken using freeze-dried yeast, is plotted in Fig. 4 (crosses). It shows that the predicted magnitude is roughly right (remember that the plot is for frozen-hydrated material so the precise agreement shown should not be taken too seriously) and the inverse-fourth-power scaling with resolution is well reproduced. Another noteworthy feature is that the plot follows a good straight line on the log-log plot all the way up to the maximum dose employed. We interpret that to mean that the resolution was not compromised by damage up to the maximum integrated dose employed. Furthermore we suggest that the eventual departure from straightness of such plots may be a good indicator of the onset of a loss of resolution due to damage. Although the data described above and plotted in Fig. 4 are typical of the majority of the data we have taken, we wish to point out that some of our data have shown scaling laws that departed significantly from inverse-fourth-power, the lowest power so far being -3.1 .

MEASUREMENT OF THE MAXIMUM TOLERABLE DOSE

Since the nineteen seventies [29], there has been strong interest in understanding the role of radiation damage in various forms of imaging of life-science samples. This has been important in direct imaging by electron and x-ray microscopes and in reconstructive imaging by methods such as the single-particle technique [30] and by x-ray and electron crystallography. During this time there has been a continual growth in the power of electron and x-ray sources and an interest in using smaller crystals in crystallography and larger numbers of images in single-particle work, all of which has generated a motivation

to push data collection to the limits allowed by damage. Thus radiation damage studies are still very much on the current agenda (see for example, the comments of Henderson [31] and the review of a recent workshop at Argonne, USA on the subject by Garman and Nave [32]). Our task to judiciously apply the latest information from these studies to the issue of determining the maximum tolerable dose for XDM.

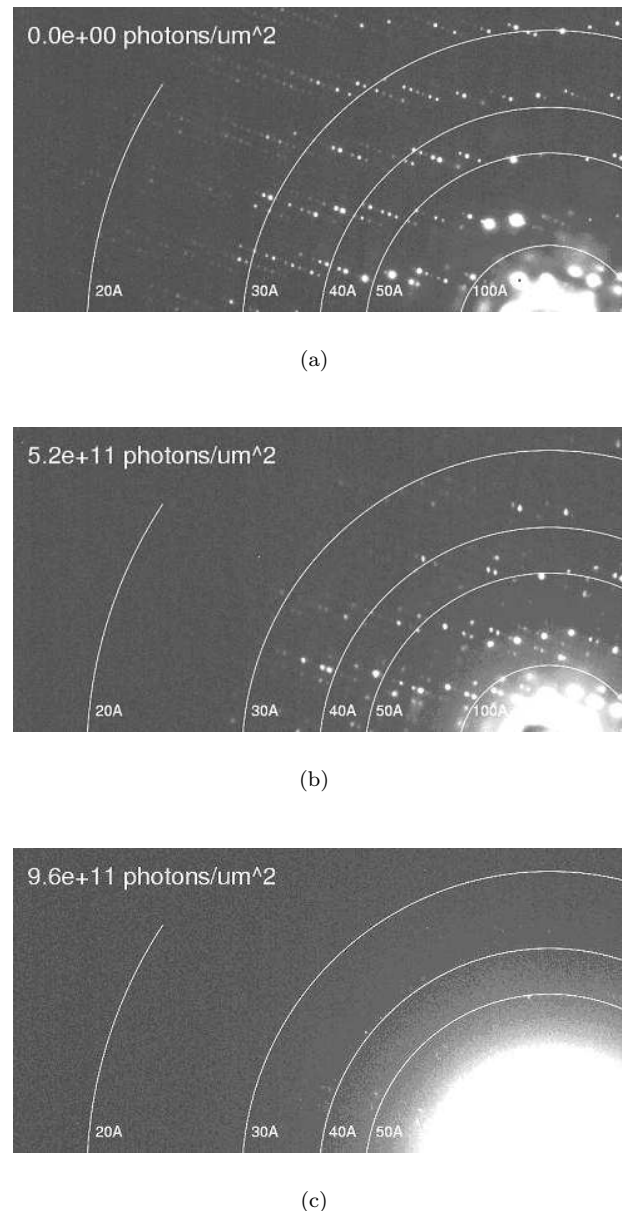


FIG. 3: Three spot patterns from the series described in the text recorded from the ribosome crystal. Many of the spots seen at the beginning of the sequence (a) have faded by the middle (b) and essentially all are gone by the end (c). The full sequence can be seen as a movie at http://bl831.als.lbl.gov/~jamesh/ribo_blast/diffraction.gif

Our resolution goal in life-science XDM is set by the considerations discussed in the introduction to be 3-10 nm. This does not correspond to the resolution goals in x-ray or electron crystallography where much higher resolution levels of 0.15-0.3 nm, that can lead to atomic-resolution structure determinations, are usually desired. In fact a significant part of the x-ray damage literature refers to *primary* damage; that is damage to the highest resolution structures. Nevertheless we have tried to find reports in the crystallography literature that have at least some reference to damage at resolution values closer to our range of interest and also give quantitative spot-fading data. We have also added information from imaging methods; electron tomography and single-particle measurements as well as a few results from XDM and x-ray microscope experiments to the compilation in Table I and Fig. 4.

Although the data from the literature noted above give quite a consistent picture as between electron and x-ray measurements (as noted by Henderson [33]), the x-ray measurements have a large gap in the resolution region of principal interest to us. This lead us to carry out spot-fading measurements ourselves using beam line 8.3.1 at the Advanced Light Source at Berkeley. The experiments were done by J. M. Holton using the established crystallography facilities of the beam line with a ribosome crystal grown by Prof. J. Cate of University of California Berkeley. The total exposure at 10 keV x-ray energy was about 24 hours with high-dose-rate (wide-slit) exposures to do damage alternated with low-dose (narrow-slit) exposures to measure the spots. The spot patterns at the beginning, middle and end of this sequence are shown in Fig. 3 and the whole process can be seen as a movie at http://bl831.als.lbl.gov/~jamesh/ribo_blast/diffraction.gif. The following points can be noted.

- The crystal has a unit cell size $a=b=693$ Å, $c=1388$ Å with space group I4122 and it diffracted out to about 10Å when it was undamaged.
- As the dose increased, the intensity of the Bragg spots faded without increase of the spot size starting from the highest-resolution spots.
- As the intensity in the (high-angle) Bragg spots diminished, that in the central (small-angle) pattern increased strongly.
- The number and resolution of the spots which faded for each increment of the dose was quantified by the DISTYL software [34] as listed in Table I and Fig. 4.
- As shown in Fig. 4 the new results are consistent with the earlier ones and, taken together, the data in the resolution range 0.1–10 nm suggest an approximate straight line on the log-log plot with

slope corresponding roughly to the linear relationship: $\text{dose(Gy)} = 10^8 \times \text{resolution(nm)}$. The data in this region are all from crystallography (electron and x-ray) and electron imaging.

We now turn to the remaining data above resolution 10 nm. There are only three data points, all coming from soft x-ray imaging experiments. Two of them differ from the other data in the sense that they represent experiments in which damage effects, meaning changes to the image with increasing dose, were not seen. These therefore represent only a lower bound on the maximum tolerable dose. In the third (the furthest to the right in Fig. 4) damage was not seen at 10^{10} Gy but was seen at 5×10^{11} Gy so that experiment did reach an end point.

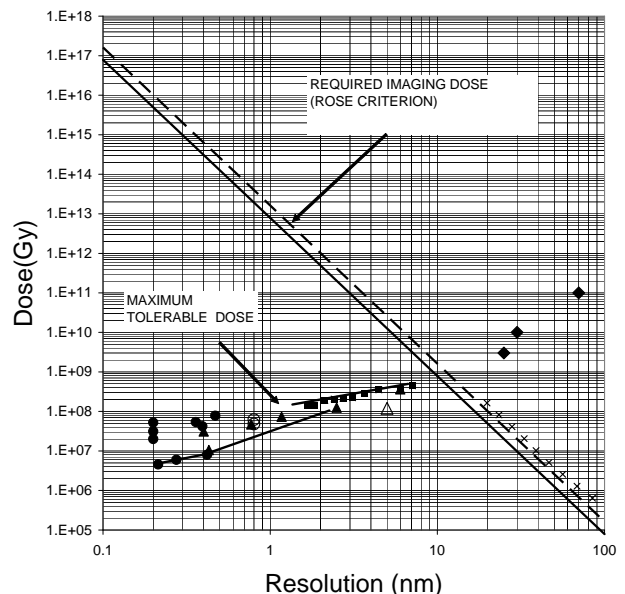


FIG. 4: graph summarizing information on the required imaging dose and the maximum tolerable dose. The reason why experiments on crystals are seen to be done successfully with around 10^8 times less than the required imaging dose is that the dose applied to a crystal is shared among at least that number of copies of the unknown object. The required imaging dose is calculated for protein of empirical formula $H_{50}C_{30}N_9O_{10}S_1$ and density 1.35 gm/cm^3 against a background of water for x-ray energies of 1 keV (solid line) and 10 keV (dashed line). Some of our measurements of imaging dose are plotted as crosses (see text). The maximum tolerable dose is obtained from a variety of experiments by ourselves and from the literature as described in Table I. The types of data from the literature are identified by the symbols as follows: filled circles: x-ray crystallography, filled triangles: electron crystallography, open circles: single-particle reconstruction, open triangles: electron tomography, diamonds: soft x-ray microscopy (including XDM), filled squares: ribosome experiment (see text).

THE MEANING OF DATA SUMMARIZED IN FIG. 4

The data summarized in Fig. 4 refer to two different dose levels; the required dose for imaging (the continuous and dashed black lines), and the maximum tolerable dose (the mostly isolated points forming a rough straight line going uphill to the right). On the left-hand side of the crossover of the two lines it is obvious that the required dose for imaging (by XDM) is far greater than the maximum tolerable dose. This reflects the fact that XDM experiments cannot be done at those resolution values. Experiments that share the dose over multiple copies of the sample (such as crystallography) have a major dose advantage and, with enough copies, such experiments can be done successfully up to the resolutions and doses indicated in Table I and Fig. 4. Obviously the dose advantage factor of crystallography compared to XDM, in which latter only a single copy of the unknown object is available, will be related to the number of copies of the unknown object contained in the crystal(s). However, one would not expect the relationship to be simple because the degree of coherent enhancement would depend in a complicated way on the experimental geometry.

Based on these understandings, the region of the graph where XDM experiments could be expected to be successful is the triangular region between the two lines to the right of the crossover. The best resolution in the “good” region is evidently at the crossover of the two “lines”. We see that this is at around 10 nm.

DISCUSSION

Initial studies [35, 36] showed that cryo-protection was quite successful in electron microscopy and crystallography and a similar technique was later adopted as a standard method in x-ray crystallography [33] where it was even more successful. The idea to extend cryo-protection to lower temperatures including liquid helium temperatures [37] has also been around for some time in the electron-microscopy community and there is some consensus that modest benefits may be obtained. The situation in the x-ray crystallography community is still much more uncertain. The Argonne workshop cited above had several papers on the subject without reaching a clear conclusion [32]. On the other hand, a recent paper by Teng and Moffat [38] assessing the range 40–150 °K provided convincing evidence that temperatures below 150 °K provide no improvement in the dose limit for *primary* radiation damage. However, they did find improvement in the dose limit for secondary and tertiary damage which is in a poorer-resolution range than primary damage. This suggests that helium temperatures might be useful for x-ray experiments in our resolution range. Although the available (non-XDM) evidence is

not unanimous on this point, we would like to explore it experimentally for XDM. However, for the moment we are only equipped for liquid-nitrogen temperature.

The work that we are doing consists of an active program of studies of yeast cells as a model sample and it is one of our goals to determine the maximum tolerable dose in that context. We are also developing the technique of measuring and reconstructing tilt series using radiation-hard samples of, for example, 50-nm gold balls [1, 2]. At the time of writing we have recorded diffraction patterns at 750 eV of freeze dried yeast and have reconstructed XDM images in 2D and stereo pair but not 3D from them. The reconstructed resolution currently achieved with freeze-dried yeast is 50 nm with a dose level of 2×10^7 Gy. With frozen-hydrated yeast we have 520 eV diffraction patterns out to 25 nm resolution but not yet a reconstruction. The freeze-dried samples were overexposed to look for signs of radiation damage. No degradation of the resolution by radiation damage was seen in this experiment although some shrinkage was observed. The shrinkage probably was a radiation effect [39] but we have not seen such shrinkage in frozen hydrated samples which are our principal interest. Although the yeast study is obviously not finished, the present paper is being submitted now in the spirit of a progress report to meet the deadline for the special issue of the journal.

CONCLUSION

Our work in this area has been directed toward understanding the resolution limit set by radiation damage in the imaging of frozen-hydrated samples using XDM. The experimental evidence we have presented here suggests that, if the maximum tolerable dose for XDM is similar to that for the other methodologies represented in Table I and Fig. 4, then we should be able to get to 10 nm resolution with “Rose-criterion” image quality. This is a prediction based on the assumptions noted, not a demonstration. At the present time this is as far as the data allow us to go in predicting the future capability of XDM. However, we believe that in the reasonably near future we will have further experimental evidence to report.

The authors are grateful to Prof. J. Cate for permission to use the ribosome crystal, to Prof. R. M. Glaeser for extended and valuable discussions and comments and to Dr. H. A. Padmore for sustained encouragement of this work. The Lawrence Berkeley National Laboratory authors and the Advanced Light source facility at Lawrence Berkeley National Laboratory are supported by the Director, Office of Energy Research, Office of Basic Energy Sciences, Materials Sciences Division of the U. S. Department of Energy, under Contract No. DE-AC03-76SF00098. The work of the LLNL authors was performed under the auspices of the U.S. Department of Energy by University of California, Lawrence Liver-

more National Laboratory under Contract W-7405-Eng-48. The Stony Brook group has been supported by National Institutes of Health grant number 1R01 GM64846-01, and by U. S. Department of Energy grant number DEFG0204ER46128.

-
- * Correspondence should be addressed to M. R. Howells, phone 510 486 4949, fax 510 486 7696: mrhowells@lbl.gov
- [1] S. Marchesini, H. N. Chapman, S. P. Hau-Riege, R. A. London, A. Szoke, H. He, M. R. Howells, H. Padmore, R. Rosen, J. C. H. Spence, U. Weierstall, *Optics Express*, **11**, 2344-2353 (2003), arXiv:physics.optics/0308064.
 - [2] S. Marchesini, H. He, H. N. Chapman, A. Noy, S. P. Hau-Riege, M. R. Howells, U. Weierstall, J. C. H. Spence, *Phys. Rev. B*, **68**, 140101(R) (2003), arXiv:physics.optics/0306174.
 - [3] J. Miao, P. Charalambous, J. Kirz, D. Sayre, *Nature*, **400**, 342-344 (1999).
 - [4] T. Beetz, C. Jacobsen, C. C. Cao, J. Kirz, O. Mentez, C. Sanches-Hanke, D. Sayre, D. Shapiro, *J. de Phys. IV*, **104**, 351-359 (2003).
 - [5] I. K. Robinson, I. A. Vartanyants, G. J. Williams, M. A. Pfeifer, J. A. Pitney, *Phys. Rev. Lett.*, **87**, 195505-1-4 (2001).
 - [6] G. J. Williams, M. A. Pfeifer, I. A. Vartanyants, I. K. Robinson, *Phys. Rev. Lett.*, **90**, 175501-1-4 (2003).
 - [7] J. Miao, T. Ishikawa, B. Johnson, E. H. Anderson, B. Lai, K. O. Hodgson, *Phys. Rev. Lett.*, **89**, 088303-1-4 (2002).
 - [8] J. Miao, H. N. Chapman, J. Kirz, D. Sayre, K. O. Hodgson, *Annu. Rev. Biophys. Biomol. Struct.*, **33**, 157-176 (2004).
 - [9] R. W. Gerchberg, W. O. Saxton, *Optik*, **25**, 237-246 (1972).
 - [10] J. R. Fienup, *Opt. Lett.*, **3**, 27-29 (1978).
 - [11] V. Elser, *J. Opt. Soc. Am. A*, **20**, 40-55 (2003).
 - [12] D. Sayre, in *Imaging Processes and Coherence in Physics*, M. Schlenker, M. Fink, J. P. Goedgebuer, C. Malgrange, J. C. Viénot, R. H. Wade, Lecture Notes in Physics, Vol. **112**, 229-235, Springer-Verlag, Berlin, 1980.
 - [13] O. Medalia, I. Weber, A. Frangakis, D. Nicastro, G. Gerisch, W. Baumeister, *Science*, **298**, 1209-1213 (2002).
 - [14] J. Plitzko, A. Frangakis, S. Nickell, F. Forster, A. Gross, W. Baumeister, *Trends in Biotechnology*, **20** (suppl), S40-S44 (2002).
 - [15] D. Sayre, J. Kirz, R. Feder, D. M. Kim, E. Spiller, *Ultramicroscopy*, **2**, 337-341 (1977).
 - [16] D. Rudolph, G. Schmahl, B. Niemann, in *Modern Microscopies*, P. J. Duke, A. G. Michette, 59-67, Pergamon, Oxford, 1990.
 - [17] C. Jacobsen, R. Medenwaldt, S. Williams, in *X-ray Microscopy and Spectromicroscopy*, J. Thieme, G. Schmahl, E. Umbach, D. Rudolph, II-93-102, Springer-Verlag, Berlin, 1998.
 - [18] D. Sayre, H. N. Chapman, *Acta. Cryst.*, **A51**, 237-252 (1995).
 - [19] Q. Shen, I. Bazarov, P. Thibault, *J. Synchrotron Rad.*, **11**, 432-438 (2004).
 - [20] R. Hegerl, W. Hoppe, *Zeitschrift für Naturforschung*, **31a**, 1717-1721 (1976).
 - [21] B. F. McEwen, K. H. Downing, R. M. Glaeser, *Ultramicroscopy*, **60**, 357-373 (1995).
 - [22] J. Kirz, C. Jacobsen, M. Howells, *Quarterly Reviews of Biophysics*, **28**, 33-130 (1995).
 - [23] J. W. Goodman, *Introduction to Fourier Optics*, MacGraw-Hill, San Francisco, 1968.
 - [24] R. Mueller, in *X-ray Laser Applications Study*, S. Jorna, (Ed Vol. **PD-LJ-76-132**, Physical Dynamics Inc, La Jolla, 1976).
 - [25] B. L. Henke, in *Proceedings of the International Conference on Low energy X-ray Diagnostics*, D. T. Attwood, B. L. Henke, Vol. **75**, 146-155, American Institute of Physics, New York, Monterey, California, 1981.
 - [26] R. A. London, M. D. Rosen, Trebes, *Appl. Opt.*, **28**, 3397-3404 (1989).
 - [27] L. Reimer, *Transmission electron microscopy: physics of image formation and microanalysis*, Springer-Verlag, Berlin, 1984.
 - [28] A. Rose, in *Advances in Electronics*, L. Marton, (Ed Vol. **1**, 131-166, New York, 1948).
 - [29] R. M. Glaeser, *Journal of Ultrastructure Research*, **36**, 466-482 (1971).
 - [30] J. Franck, *Three-Dimensional Electron Microscopy of Macromolecular Assemblies*, Academic Press, San Diego, 1996.
 - [31] R. Henderson, *Quarterly Reviews of Biophysics*, **37**, 3-13 (2004).
 - [32] E. Garman, C. Nave, *J. Synchrotron Rad.*, **9**, 327-328 (2002).
 - [33] R. Henderson, *Proceedings of the Royal Society of London*, **B 241**, 6-8 (1990).
 - [34] Z. Zhang, Private communication, 2004.
 - [35] R. M. Glaeser, K. A. Taylor, *Journal of Microscopy*, **112**, 127-138 (1978).
 - [36] S. B. Hayward, R. M. Glaeser, *Ultramicroscopy*, **4**, 201-210 (1979).
 - [37] J. Dubochet, E. Knapek, I. Dietrich, *Ultramicroscopy*, **6**, 77-80 (1981).
 - [38] T.-Y. Teng, K. Moffat, *J. Synchrotron Rad.*, **9**, 198-201 (2002).
 - [39] J. Berriman, K. R. Leonard, *Ultramicroscopy*, **19**, 349-366 (1986).
 - [40] R. M. Glaeser, Private communication, 2004.
 - [41] G. Schneider, *Ultramicroscopy*, **75**, 85-104 (1998).
 - [42] J. Maser, A. Osanna, Y. Wang, C. Jacobsen, J. Kirz, S. Spector, B. Winn, D. Tennant, *Journal of Microscopy*, **197**, 68-79 (2000).
 - [43] W. P. Burmeister, *Acta Cryst.*, **D56**, 328-341 (2000).
 - [44] P. Sliz, S. C. Harrison, G. Rosenbaum, *Structure*, **11**, 13-19 (2003).
 - [45] R. Glaeser, M. Faciotti, P. Walian, S. Rouhani, J. Holton, A. Macdowell, R. Celestre, D. Cambie, H. Padmore, *Bio-physical J.*, **78**, 3178-3185 (2000).

Res'n (nm)	Dose (Gy)	Experiment	Particle energy (keV)	Reference	Sample: (crystal where stated)
Electrons					
0.43	1.06E+07	spot fading	100	[35]	catalase
2.5	1.25E+08	spot fading	100	[35]	catalase
5.0	1.20E+08	tomography	300	[13, 14]	cell in amorphous ice
0.77	4.67E+07	spot fading	100	[36]	purple membrane
1.17	7.35E+07	spot fading	100	[36]	purple membrane
0.4	3.12E+07	spot fading	100	[36]	purple membrane
0.8	4.80E+07	single particle reconst'n	100	[40]	protein single molecules
0.8	6.20E+07	single particle reconst'n	100	[40]	protein single molecules
X-rays					
30	1.00E+10	microscopy Berlin	0.52	[41]	cell in amorphous ice
60	5.00E+11	microscopy Brookhaven	0.52	[42]	cell in amorphous ice
0.2	2.00E+07	generic limit	8-12	[33]	organic material
0.2	3.10E+07	spot fading	13.1	[43]	myrosinase
0.36	5.40E+07	spot fading	12.4	[44]	various
0.47	7.80E+07	spot fading	12.4	[44]	various
0.39	4.20E+07	spot fading	12.4	[44]	various
25.0	3.00E+09	XDM Berkeley	0.52	this work	yeast cell freeze dried
0.42	8.00E+06	spot fading	11	[45]	bacteriorhodopsin
0.28	5.95E+06	spot fading	11	[45]	bacteriorhodopsin
0.21	4.55E+06	spot fading	11	[45]	bacteriorhodopsin
7.1	4.44E+08	spot fading	10	this work	ribosome
6.0	3.64E+08	spot fading	10	this work	ribosome
4.5	3.49E+08	spot fading	10	this work	ribosome
3.7	2.85E+08	spot fading	10	this work	ribosome
3.1	2.22E+08	spot fading	10	this work	ribosome
2.7	2.14E+08	spot fading	10	this work	ribosome
2.4	2.06E+08	spot fading	10	this work	ribosome
2.1	1.90E+08	spot fading	10	this work	ribosome
1.8	1.43E+08	spot fading	10	this work	ribosome
1.7	1.43E+08	spot fading	10	this work	ribosome

TABLE I: data types and sources used to estimate the maximum tolerable dose